Non-Invasive Plasma Diagnostic Inside A Hall Thruster Discharge

IEPC-2007-69

Presented at the 30th *International Electric Propulsion Conference, Florence, Italy*
September 17-20, 2007

Rostislav Spektor* and Edward J. Beiting†

A small optical probe that can be translated longitudinally inside the outer insulating wall of a Hall thruster is used to investigate spectroscopic emission of the plasma discharge. Electron temperature inside the discharge channel is inferred from the spectroscopic emission using an advanced collisional-radiative model that includes the effects of metastable states. Moving the probe along the discharge channel produces axially-resolved temperature profiles. Additionally, electron temperature profiles in the plume, up to $100\ mm$ **from the thruster exit, are obtained using a fiber optic-based collection system. Results of the spectroscopic analysis are found to be consistent with previous invasive probe measurements. They show that the maximum electron temperature increases with the discharge voltage and moves toward the thruster exit. Measurement accuracy is found to be greatly affected by the uncertainty in spectroscopic calibration.**

Nomenclature

T_e	= electron temperature
T_e^{max}	= maximum electron temperature
V_d	= discharge voltage
I^{dat}	= acquired line intensity
I^{mod}	= modeled line intensity
χ^2	= fitting norm
i	= summation index
j	= summation index
HCT	= Hall Current Thruster
$EEDF$	= Electron Energy Distribution Function
CRM	= Collisional-Radiative Model
CCD	= Charge Coupled Device

*Member of Technical Staff, The Aerospace Corporation, rostislav.spektor@aero.org
†Senior Scientist, The Aerospace Corporation, edward.j.beiting@aero.org

I. Introduction

Hall Current Thrusters (HCTs) are space plasma propulsion devices that rely on axial electric field to accelerate ions. Electric field profile, $E_z(z)$, inside the thruster is established by electrons, which flow from the external cathode to the anode, and are trapped in the annular discharge channel by applied radial magnetic field, $B_r(z)$, long enough to ionize propellant gas. The combination of axial electric and radial magnetic fields results in primarily azimuthal electron drift proportional to E_z/B_r. The axial electron flow depends on collision frequency with heavy species, thruster walls, and propagating electromagnetic fluctuations. Consequently, electron transport plays critical role in thruster operation. Electron temperature measurements are essential for understanding electron transport.

Electron temperature in an HCT is typically measured with Langmuir or floating probes.[1,2] While simple, this invasive technique contains inherent measurement errors caused by plasma interaction with the surface of the probe. Furthermore, extreme conditions in the discharge plasma impose severe restrictions on probe survivability. To overcome these limitations, a fast-moving probe can be used to measure electron temperature distribution inside a thruster.[3,4]

An alternative approach is to use a non-invasive, optical technique.[5,6] Optical techniques allow accurate measurements, with spatial resolution of about 1 mm, without perturbing the plasma. In the last decade optical investigation of the HCT plasma has seen rapid development. Kusamoto *et al.*[7] and Meezan *et al.*[8] investigated oscillation of the optical spectra to study electron transport. Leray *et al.*[9] employed a simple Collisional-Radiative Model (CRM) to investigate plasma density and Electron Energy Distribution Function (EEDF) inside an SPT-50 thruster. Karabadzhak *et al.* developed a more involved method of determining electron temperature in a series of articles published between 2001 and 2006.[10–12] This model has been successfully applied by Sommerville and King[13] and Matlock *et al.*[14] to investigate various types of HCTs.

In the previous studies a series of small holes was drilled in the thruster wall in order to optically access various positions inside the thruster. This method restricts measurements to only few predefined points. In this paper we propose an alternative method involving a small quartz probe moving inside a small channel that is drilled in the ceramic insulator. This method allows accurate spectroscopic measurements at an arbitrary position inside the thruster channel.

This paper is organized as follows. In Section II we briefly describe the Near Field facility and the 2kW GPT-1 HCT used in this experiment. In Section III we give a detailed description of the quartz probe, which was used to obtain internal spectroscopic measurements. We also briefly describe the fiber optic-based collection optics used to investigate the thruster plume. We then present and analyze collected data in Section IV. Influence of various error sources on the overall measurement uncertainty is discussed in Section V. Finally, we summarize our findings and propose future avenue for improvement in Section VI.

II. Experimental Setup

Investigations reported in this paper were conducted in the Near Field facility at The Aerospace Corporation. The facility comprises a 3 m long and 1.5 m diameter stainless steel chamber, shown schematically in Fig. 1. The chamber is pumped by two He-cooled nude sails with the speed of $\sim 42,000$ l/s. Cooling of the sails is maintained by two CVI CBST 6.0 compressors through expander heads. Additionally, a liquid nitrogen shroud helps maintaining the low-temperature environment inside the tank. Before the cryogenic system is turned on, the chamber is pumped down to a roughing pressure of ~ 150 mTorr with a combination of a 412H Stokes mechanical pump and a blower (not shown in Fig. 1). Two copper panels, cooled by liquid nitrogen (LN_2), are installed in front of the He sails. The cryo-panels are designed to screen the sails from the thruster beam. The side of the panel facing the thruster is covered with carbon velvet (or felt) to reduce sputtering. Carbon felt is also used on a circular panel covering the back wall of the chamber. The velvet was applied to each copper cryo-panel (the back circular panel was assembled from quarter panels) by Energy

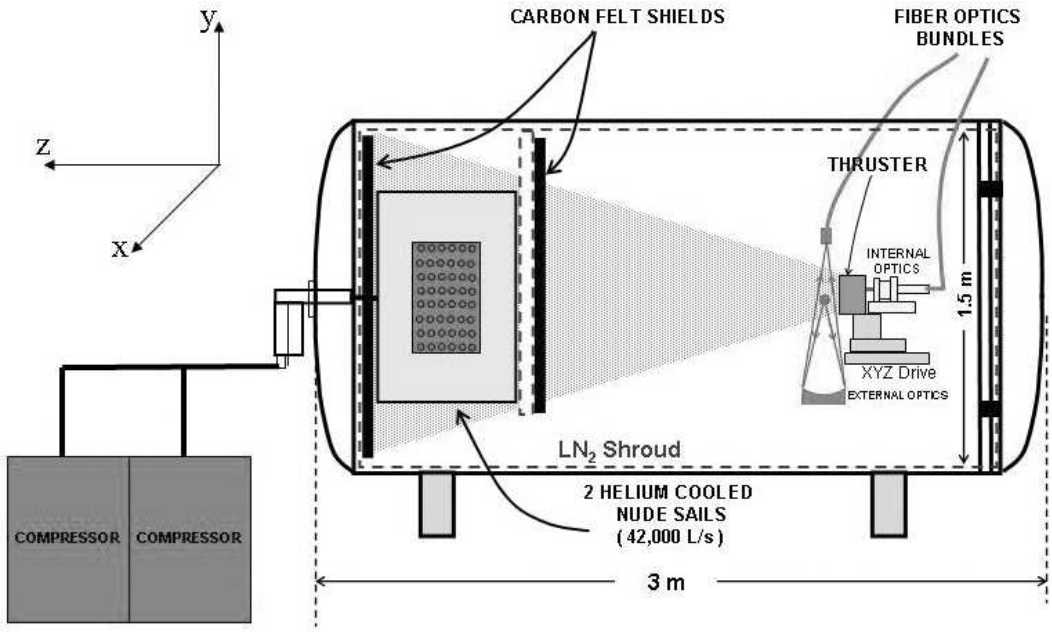

Figure 1. Schematic of the Near Field facility showing He sails, liquid nitrogen shroud, thruster, and external optics.

Sciences Laboratories, INC., San Diego, Ca. The velvet has approximately 10% the sputter rate of carbon when ions strike the sheet orthogonally (i.e. parallel to the fibers). Measurements indicate that there is less than $1^0 K$ temperature gradient between the copper surface and tips of the fibers at LN_2 temperatures.[15]

The system is capable of maintaining a base pressure of $5 \cdot 10^{-7}\ Torr$, but with the thruster running, pressure can increase up to $2 \cdot 10^{-5}\ Torr$, as measured by the ionization gauge mounted on the side of the chamber next to the thruster.

For experiments reported in this paper we used the GPT-1 thruster – a 2 kW Hall thruster built by General Plasma Technology INC, shown in Fig. 2. The thruster is similar in design to the thruster investigated by Raitses *et al*. in Ref. [16]. The outer and inner diameters of the discharge channel are $12.3\ cm$ and $7.3\ cm$ respectively, while the channel length is $4.2\ cm$. Channel walls are made from the combat HP grade boron nitride. The same material is also used for the center plug of the thruster. The thruster has an inner and outer coils for creating mainly radial magnetic field. Additionally, there is a trim coil that is similar to the outer coil, and is located behind it. This coil can be used to create a cusp in the magnetic field. The trim coil, however, was not used for the experiments described in this paper. The thruster uses a standard Heatwave HWPES-250 hollow cathode.

Spectroscopic data was obtained for thruster discharge voltages ranging between 200 and 350 Volts, and discharge currents between 1.6 and 2.1 Amperes respectively. Stable thruster operation was chosen by adjusting magnetic field to minimize the discharge current. The anode flow rate was set at 19 sccm while the cathode flow rate was set at 2 sccm.

The thruster was placed on the opposite side of the chamber from the sails, on a motorized platform that can be translated in three orthogonal directinos ("xyz drive" in Fig. 1). The xyz drive allows us to measure electron temperature distribution in the plume by moving the thruster relative to a stationary external collection optics. For the experiments reported in this paper the xyz drive was moved $\sim 10\ cm\ (4\ in)$ along z direction.

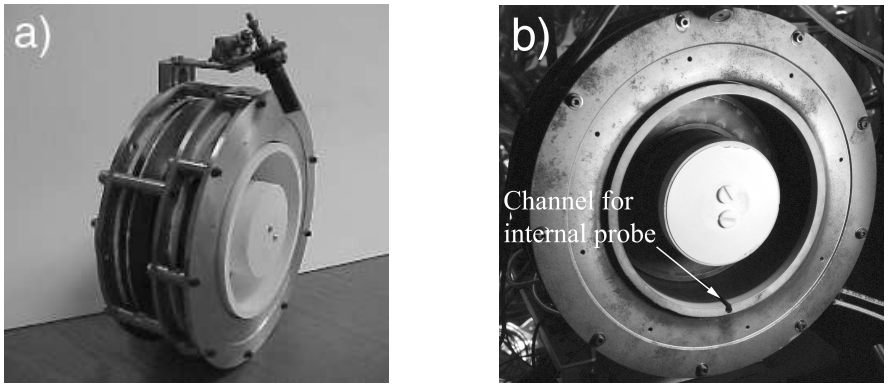

Figure 2. Photographs of the 2 kW Hall thruster built by General Plasma Technology LLC. The left picture shows the outer and trim magnet coils as well as the hollow cathode. Thruster walls are made from the combat HP grade boron nitride. Same material is also used as the center plug. The right picture shows the quartz probe channel drilled at the bottom of the outer wall.

III. Optical Diagnostics

In order to measure optical spectra inside the thruster we machined a small ($4\ mm$ diameter) channel inside the boron nitride insulator, as shown in Fig. 2b. The channel creates a $3.3\ mm$ opening in the insulator to allow collection of light by the quartz probe. The probe is $178\ mm$ long and $3.3\ mm$ in diameter, as shown schematically in Fig. 3. It is inserted from the back of the thruster, and is moved along the channel by a motorized translation stage to any point from just behind the anode to $8\ mm$ outside the thruster exit.

Using a snap connector, the probe is attached to a fiber optic cable bundle that leads through a vacuum feed-through to SPEX 1870 $0.5\ m$ spectrometer. Data acquisition is performed with a Princeton Instruments SpectruMM:250B CCD camera (1024×252 pixels), which is controlled by the WinSpec software.

The front end of the probe was polished flat, creating a square $2\ mm \times 2\ mm$ viewing area, as shown in Fig. 3. Radially opposite to this viewing area, the tip of the probe is cut at 38^0 to create total internal reflection of the light impacting the probe perpendicularly to the flattened viewing area. Additionally, a layer of silver was deposited on top of the angled surface to improve light reflection. Furthermore, the surface of the probe, excluding the viewing area, was coated with a layer of aluminum in order to avoid excessive electron flux. However, we noticed that after about 20 hours of thruster operation this layer, as well as the silver coating at the tip, were etched away by the plasma without damaging the probe itself.

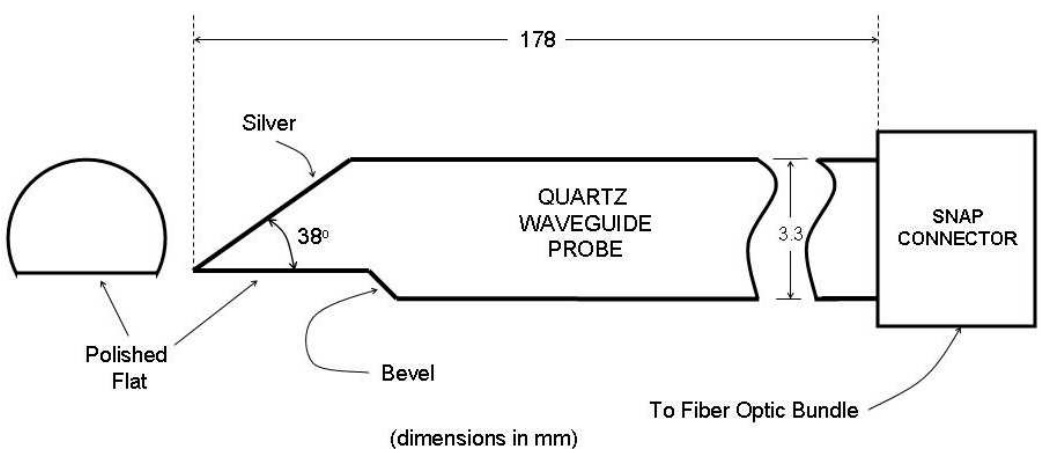

Figure 3. Schematic of the quartz probe used to investigate optical spectra of the plasma inside HCT. Light is collected by the flat area at the tip of the probe and is guided toward the snap connector, were the probe is attached to a fiber optic cable.

Before electron temperature inferred from the probe data can be trusted it is important to ensure that the steady-state plasma properties are not altered in the presence of the probe. While the total area of the probe exposed to the plasma is a small fraction of the outer thruster wall, the probe can alter discharge parameters locally by affecting the sheath. Multiple authors discussed importance of the wall sheath and Secondary Electron Emissions (SEE) for the HCT operation.[17–19] Dunaevsky *et al.*[19] measured the total yield of the secondary electron emission as a function of electron energy below 100 eV for quartz and combat HP grade boron nitride, which is used in the GPT-1 thruster. Their findings indicate that both boron nitride and quartz have similar SEE characteristics. For example, the energy at which the SEE yield equals to one is 30 to 40 eV (depending on the fitting model) for boron nitride and 30 to 45 eV for quartz. Therefore, introduction of the quartz probe does not alter plasma sheath significantly, and local measurements taken by the quartz probe are indicative of the overall plasma properties at a given axial position. We also assume for these measurements that EEDF is Maxwellian and that inside the thruster electron temperature does not vary radially. As discussed by Morozov,[1] Keidar,[20] and others, this is a valid assumption since the radial electron energy quickly reaches an equilibrium in the presence of radial magnetic field, leading to the concept of "thermalized potential".

In addition to the described internal optical probe, we designed external collection optics to measure thruster plume spectra. This external optical collection system comprises a $15\ cm$ concave mirror that focuses light from a point in the thruster plume onto a $2\ mm$ diameter fiber optic cable, as shown on the right of Fig. 1. Electron temperature distribution in the plume can be measured by moving the thruster with the xyz drive. Thus, external collection optics together with the internal probe allows us to construct continuous electron temperature profile from the anode to $\sim 10\ cm$ away from the thruster exit.

The external collection optical setup was chosen based on the physical limitations of the chamber, and designed to maximize collected light. A setup consisting of a lens mounted externally to the chamber and collecting light through a port window was also tested but produced a signal with much smaller signal to noise ratio.

IV. Data Analysis and Discussion

We collected four data sets at 200, 250, 300, and 350 V, all at the same flow rate and magnetic field configuration as described in Section II. Data consisted of intensity measurements of eight XeI lines (788.7 nm, 823.2 nm, 828.0 nm, 834.7 nm, 881.9 nm, 904.5 nm, 916.3 nm, and 980.0 nm) taken at various positions along z axis, inside the thruster with the quartz probe, and outside of the thruster with the external collection optics. Electron temperature profiles deduced from two of these sets (200 and 250 V) are shown in Fig. 4. The measurements were taken at intervals of $5\ mm$ inside the thruster, and $0.5\ in$ ($12.7\ mm$) in the plume. Data points taken with the internal probe are indicated by open symbols, while data points taken with the external optics are represented by the filled symbols. Electron temperature profiles measured with a tungsten probe by the HTX (Hall Thruster Experiment) group at Princeton Plasma Physics Laboratory[16,21] are also shown in Fig. 4 for comparison (continuous curves). It is important to note that the tungsten probe data was obtained for a thruster similar, but different from the GPT-1, and therefore, exact data match was not expected.

We used two collisional-radiative models to analyze the spectroscopic data. First, we obtained electron temperature profiles using a model developed by Karabadzhak *et al.*[12] This model analyzes all eight collected spectroscopic lines, and thus includes the effects of metastable atomic states, which were shown to have an important contribution to the CRM analysis. Electron temperature profiles deduced from this model are shown by circles in both panels of Fig. 4. Additionally, we analyzed data with a simple CRM model that does not take into account metastable states. For this model only three lines with small metastable state population were used: 788.7 nm, 828.0 nm, and 834.7 nm. This simple model is less accurate than the first model, since two of these lines (788.7 nm and 834.7 nm) are weak. Furthermore, it has been shown that this simple CRM analysis leads to reduced electron temperature predictions.[12] This conclusion is indeed

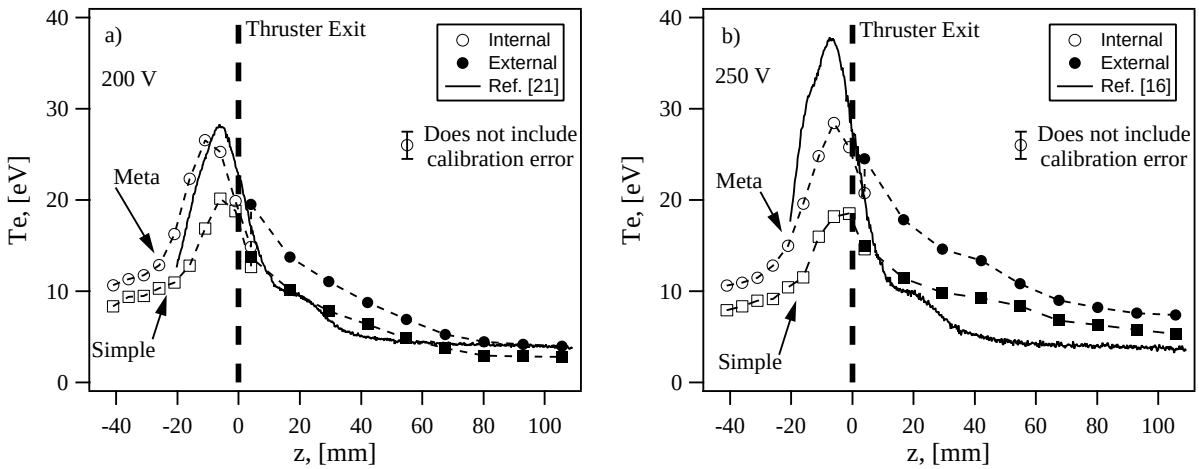

Figure 4. Electron temperature profiles deduced from the spectroscopic data. Electron temperature profiles obtained with the model developed in Ref. [12], which relies on all nine lines, are indicated as "Meta", while results of the simple CRM model are shown by the "Simple" curves. Data collected by the HTX group[16,21] are shown by solid curves. Panel a) shows the 200 V data, while panel b) shows the 250 V data.

supported by our data, as can bee seen from Fig. 4, which compares results of the simple CRM analysis ("Simple") to those obtained from the model that takes into account metastable states ("Meta").

Electron temperature at $z = 5\,mm$ was measured with both the internal probe and external collection optics for comparison. As can be seen from Fig. 4, at this position the external and internal data analyzed with the metastable CRM analysis produced significantly different temperature predictions. The simple CRM analysis, on the other hand, produced a much better match between the external and internal measurements.

Possible sources of discrepancy in the metastable CRM analysis will be discussed in the next section. It is interesting to note, however, that for the 250 V data set the external optics measurements seem to consistently *over-predict* electron temperature when compared to the results obtained by the HTX group. The 200 V data also shows similar disagreement for the points between the thruster exit and $z \sim 80\,mm$. Inside the thruster the disagreement trend is opposite. While, the 200 V data shows good agreement between the optical and invasive measurements, the higher voltage optical data, exemplified by the 250 V data set in Fig. 4b, consistently *under-predicts* electron temperature when compared to the results obtained by the HTX group. As will be described in the next section, both the internal and external data disagreements may be explained by inaccuracies in the spectroscopic intensity calibration.

One result common to both optical and invasive measurements is the location of the maximum electron temperature as a function of the discharge voltage – our measurements are consistent with previous finding that temperature peak moves closer to the thruster exit as the discharge voltage is increased. Additionally, our spectroscopic measurements show that from 200 to 350 Volts the maximum electron temperature increases together with discharge voltage. In particular, a linear fit through the data points ($T_e^{max} \sim 0.08 \cdot V_d$) produces a proportionality factor consistent with results reported by Kim[22] ($T_e^{max} = 0.07 - 0.09 \cdot V_d$), as shown in Fig. 5. Future studies will show if the maximum electron temperature saturates at higher discharge voltages.[23]

V. Error Analysis

Uncertainty in electron temperature determined from the spectroscopic measurements is produced by random errors, associated with repeatability, and by systematic errors, which are caused by spatial resolution, imperfect calibration of the measuring equipment, and model simplifications. In this section we discuss and

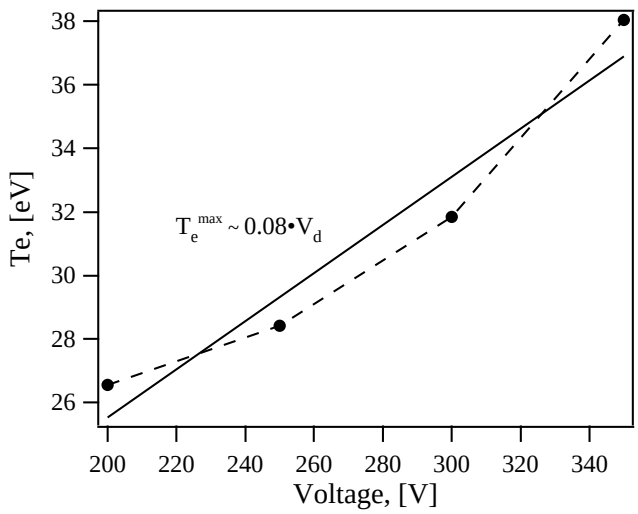

Figure 5. Maximum electron temperature as a function of discharge voltage. The maximum temperature increases with the discharge voltage. A linear fit to the measured data produces proportionality factor consistent with the results reported by Kim.[22]

quantify these errors to show that spectroscopic diagnostic technique can yield highly accurate electron temperature measurements.

We found that data reproducibility uncertainty introduced one of the smallest components to the overall measurement error. The standard deviation in the scatter of multiple electron temperature predictions, measured at the same physical location was below 3%.

Spatial resolution is the second smallest uncertainty component. This uncertainty comes about because of the gradients in plasma density and electron temperature. For a given spectral line the signal delivered to spectrometer is a convolution of light coming from point sources, which are spread inside a small volume with the center at the focal point. A point farthest from the focal point will typically have the smallest contribution to the signal. However, if significant gradients exist within this volume, points far from the focal point may have a large contribution to the line intensity. The overall effect in this case will be a signal, which is inconsistent with the Maxwellian electron energy distribution, assumed by the CRM analysis.

We investigated the spatial uncertainty of the external optics by placing a point light source at the focal point, moving the source around, and observing the signal intensity drop off. As expected, in x and z direction spatial resolution was limited by the diameter of the fiber optic cable. Within $1\ mm$ from the focal point the signal intensity dropped by 50%. Combining this with the maximum expected temperature gradient of $\sim 2\ eV/mm$, approximated from the measured values, we obtain $\sim 2.6\%$ in the measurement uncertainty. In y direction the signal intensity is not limited by the fiber diameter, but rather by the speed of the optics. Because light intensity collected away from the focal point drops off quicker for smaller f-numbers, faster optical setup is more accurate. Experimentation with the moving point source yielded uncertainty of $\sim 3\%$. Similar investigation was done for the internal probe. We, therefore, take the total uncertainty due to spatial resolution as 3%.

As was mentioned earlier, CRM models tend to under-predict electron temperature. The advanced CRM model developed by Karabadzhak[12] *et al.* , produces much closer agreement with the data. One limitation common to CRM models is that relative line intensities become less sensitive to electron temperature at $T_e \gtrsim 20$ eV than at the lower values of T_e, as shown by Fig. 3 in Ref. [12]. Thus, the uncertainty due to this inherent model limitation increases with electron temperature. One way to mitigate this uncertainty is to analyze larger number of lines. The reason why the advanced model developed by Karabadzhak *et al.* is more accurate than typical CRM models is that it allows inclusion of the lines with significant metastable

population. Based on the analysis presented in Ref. [12] we place the uncertainty due to the model limitation at 10%.

Furthermore, at high electron temperatures Ref. [12] reports that the model diverged without producing an accurate line fit. The model finds a solution by minimizing a norm χ^2, which is the least-squared difference between the measured and modeled line intensities. We experienced a similar divergence problem close to the thruster exit, where electron temperature is high. Consequently we developed a different form of metric to fit the spectroscopic data,

$$\chi^2 = \sum_i \sum_{j<i} \frac{\left([I_i^{mod}/I_j^{mod}] - [I_i^{dat}/I_j^{dat}]\right)^2}{[I_i^{dat}/I_j^{dat}]^2},$$

where i and j run over the collected spectral lines, I^{mod} is the modeled line intensity, while I^{dat} is the measured line intensity. For the data reported in this paper, the new metric has always produced a convergent result.

The final, and the largest contribution to the uncertainty comes from calibration of the optical setup. Calibration was performed separately for the quartz probe and the external collection optics with a tungsten light source. The source temperature was measured by optical pyrometer with an accuracy of $\pm 500\ K$. The range of an individual spectroscopic measurement ($25\ nm$) was limited by the size of the CCD camera. Therefore, multiple shots were stitched together to obtain continuous spectral response of the instrument. This procedure introduced the largest error in our measurements. We found that variation in calibration curves obtained at exactly the same conditions can produce an error in electron temperature as high as 30%. It is important to remember that this is a bias error, producing a shift of the entire temperature profile. Therefore, uncertainty in calibration can explain the disagreement between the external and internal measurements, as well as with the HTX probe data at high discharge voltages.

We believe that replacing spectrometer with a spectrograph that allows us to measure all Xe lines in one span will reduce this error source, if not eliminate it entirely. Because we believe that this error can be eliminated, we do not include it in the overall error assessment. Assuming that all described error sources are independent, we finally can estimate the overall measurement error to be 11%.

VI. Conclusions

This paper presented the inaugural measurements from a new compact electric propulsion diagnostic facility at The Aerospace Corporation. We designed and tested a new non-invasive diagnostic for measuring electron temperature profiles inside a Hall thruster discharge. Additionally, we measured electron temperature profiles in the near-field plume of the thruster using a fiber optic-based collection system. Thus, combining the discharge and plume profiles we obtained continuous electron temperature distribution spanning from the anode to $\sim 100\ mm$ outside the thruster exit.

We collected and analyzed data at various discharge voltages and compared the resultant electron profiles with data collected by a tungsten probe for similar thruster conditions. At $200\ V$ the agreement between the invasive and optical profiles was satisfactory. At higher discharge voltages there was a significant disagreement between the two techniques. This disagreement may be explained by poor spectroscopic calibration accuracy. Calibration accuracy may also explain disagreement between the external and internal measurements. We believe that the calibration accuracy can be significantly improved, and the overall measurement error may be as small as 11%.

Additionally we found that trends in the collected data were consistent with previously reported results. For example, the maximum electron temperature increased with the discharge voltage, with the proportionality factor of 0.08. Furthermore, location of the maximum electron temperature moved toward the thruster exit as discharge voltage was increased. These initial results are interim and their accuracy will be increased as new instrumentation is added

Acknowledgements

The authors thank Yevgeny Raitses for multiple insightful comments and discussions. The project was supported by The Aerospace Corporation through its Independent Research and Development Program.

All trademarks, service marks, and trade names are the property of their respective owners.

References

[1]Morozov, A. and V.V., S., "Fundamentals of Stationary Plasma Thruster Theory." *Rev. Plasma. Phys.*, Vol. 21, February 2000, pp. 203.

[2]Smirnov, A., Raitses, Y., and Fisch, N. J., "Plasma measurements in a 100 W cylindrical Hall thruster," *J. Appl. Phys.*, Vol. 95, No. 5, March 2004, pp. 2283.

[3]Staack, D., Raitses, Y., and Fisch, N. J., "Shielded electrostatic probe for nonperturbing plasma measurements in Hall thrusters," *Rev. Sci.Instrum*, Vol. 75, No. 2, February 2004, pp. 393–399.

[4]Linnella, J. A. and Gallimore, A. D., "Internal plasma potential measurements of a Hall thruster using plasma lens focusing," *Phys.Plasmas*, Vol. 13, 2006.

[5]Hutchinson, I., *Principles of Plasma Diagnostics*, Cambridge University Press, Cambridge, United Kingdom, 2nd ed., 2002.

[6]Colonna, G., Pietanza, L., and Capitelli, M., "A collisional radiative model for Xe electrical thrusters," Presented at the 31th AIAA Plasmadynamcs and Lasers Conference, Denver, Co, 19-22 June, 2000.

[7]Kusamoto, D. and Komurasaki., K., "Optical Diagnosis of Plasma in a Channel of Hall Thrusters." Presented at the 25th International Electric Propulsion Conference (IEPC), Cleveland, Ohio, August 24-28, 1997. IEPC-97-067.

[8]Meezan, N. B., Hargus, J. W. A., Schmidt, D. P., and Cappelli, M. A., "Optical Study of Anomalous Electron Transport in a Laboratory Hall Thruster," Presented at the 35th AIAA/ASME/SAE/ASEE Joint Propulsion Conference (JPC), Los Angeles, California, 1999.

[9]Leray, P., Bonnet, J., and Pigache, D., "Spatially Resolved Emission Spectroscopy along a SPT Channel. Interprctation of Data by a Collisional-Radiative Model." Presented at the 25th International Electric Propulsion Conference (IEPC), Cleveland, Ohio, August 24-28, 1997. IEPC-97-054.

[10]Karabadzhak, G. F., Chiu, Y.-H., Williams, S., and Dressler, R. A., "Hall thruster optical emission analysis based on single collision," Presented at the 37th AIAA/ASME/SAE/ASEE Joint Propulsion Conference (JPC), Salt Lake City, Utah, 8-11 July, 2001.

[11]Chiu, Y., Austin, B., Williams, S., Dressler, R., and Karabadzhak, G., "Passive optical diagnostic of Xe-propelled Hall thrusters. I. Emission cross sections," *J. Appl. Phys.*, Vol. 99, 2006.

[12]Karabadzhak, G., Chiu, Y., and Dressler, R., "Passive optical diagnostic of Xe-propelled Hall thrusters. II. Collisional-radiative model," *J. Appl. Phys.*, Vol. 99, 2006.

[13]Sommerville, J. and King, L., "An Optical Diagnostic for Xenon Hall THrusters Including Metastable Contributions," Presented at the 42th AIAA/ASME/SAE/ASEE Joint Propulsion Conference (JPC), Sacramento, Ca, 9-12 July, 2006, AIAA-2006-4823.

[14]Matlock, T., Jr., W. H., Larson, C., and Nakles, M., "An Inversion Method for Reconstructing Hall Thruster Plume Parameters from Line Integrated Measurements," Presented at the 43th AIAA/ASME/SAE/ASEE Joint Propulsion Conference (JPC), 2007, Cincinnati, OH, 8-11, July 2007, AIAA-2006-4823.

[15]Private communication with T. Knowles, Energy Sciences Laboratories, INC., San Diego, Ca.

[16]Raitses, Y., Staack, D., Keidar, M., and Fisch, N. J., "Electron-wall interaction in Hall thrusters," *Phys.Plasmas*, Vol. 12, May 2005, pp. 057104.

[17]Hobbs, G. D. and Wesson, J. A., "Heat flow through a Langmuir sheath in the presence of electron emission," *Plasma Phys.*, Vol. 9, 1967, pp. 85.

[18]Choueiri, E. Y., "Fundamental Difference between the Two Hall Thruster Variants," *Phys.Plasmas*, Vol. 8, 2001, pp. 5025.

[19]Dunaevsky, A., Raitses, Y., and Fisch, N. J., "Secondary electron emission from dielectric materials of a Hall thruster with segmented electrodes," *Phys.Plasmas*, Vol. 10, No. 6, June 2003, pp. 2574.

[20]Keidar, M., Boyd, I., and Parrilla, J., "Modeling of the Plasma Flow in High-Power TAL," Presented at the 39th AIAA/ASME/SAE/ASEE Joint Propulsion Conference (JPC), 2003, Huntsville, AL, 20-23, July 2007, AIAA-2003-4701.

[21]Generously provided to us by Y. Raitses and the HTX group.

[22]Kim, V., *J. Propul. Power*, Vol. 14, 1998, pp. 736.

[23]Raitses, Y., Staack, D., Smirnov, A., and Fisch, N. J., "Space charge saturated sheath regime and electron temperature saturation in Hall thrusters," *Phys.Plasmas*, Vol. 12, July 2005, pp. 073507.